Astragaloside IV targets TUBB4B to inhibit proliferation and promote apoptosis of pituitary tumor cells via the STMN1/ERK pathway

JIALE LI[1,2], YUFEI QU[1,2], WENGE ZHANG[1,2], ZEXU YANG[2,3], YANGDONG ZENG[1,2], JISHENG XU[1,2], KUNCEN XIE[1,2] and QI LIU[1]

[1]Department of Neurosurgery, The First Affiliated Hospital of Shihezi University, Shihezi University, Shihezi, Xinjiang 832008, P.R. China; [2]National Health Commission Key Laboratory of Prevention and Treatment of Central Asia High Incidence Diseases (Co-construction), Shihezi University, Shihezi, Xinjiang 832008, P.R. China; [3]Department of Ultrasound Medicine, The First Affiliated Hospital of Shihezi University, Shihezi University, Shihezi, Xinjiang 832008, P.R. China

Received November 7, 2025; Accepted March 13, 2026

DOI: 10.3892/ijmm.2026.5822

Abstract. Pituitary tumors, as common intracranial neoplasms, present challenges in clinical management because of high postoperative recurrence rate, drug resistance and pronounced side effects. Astragaloside IV (AS-IV), the primary active component of the traditional Chinese herb *Astragalus membranaceus*, has antitumor activity in numerous types of cancer. However, its effects and mechanisms in pituitary tumors remain unclear. The present study aimed to investigate the effects of AS-IV on proliferation and apoptosis of pituitary tumor cells and to elucidate its molecular mechanisms. Cell Counting Kit-8 (CCK-8), TUNEL, EdU, immunohistochemistry (IHC), and Western blotting, among others, showed that AS-IV significantly suppressed the viability of the rat pituitary tumor cell lines GH3 and MMQ in a concentration- and time-dependent manner while inducing apoptosis. Tubulin β4B Class IVb (TUBB4B) was highly expressed in pituitary tumor tissue and its overexpression promoted cell proliferation while inhibiting apoptosis. AS-IV bound TUBB4B with high affinity, forming a stable complex. TUBB4B regulation influenced pituitary tumor cell sensitivity to AS-IV, with AS-IV demonstrating enhanced antitumor efficacy in TUBB4B-overexpressing tumors. TUBB4B activated the ERK/MAPK signaling pathway by upregulating Stathmin 1 (STMN1) expression, which promoted G1/S phase transition. The ERK-specific inhibitor U0126 reversed this pro-proliferative effect. To the best of our knowledge, the present study is the first to reveal that AS-IV inhibits pituitary tumor proliferation and promotes apoptosis by targeting TUBB4B to regulate the STMN1-ERK signaling axis, providing a novel theoretical basis and potential strategies for traditional Chinese medicine treatment and molecular targeted research on pituitary tumors.

Correspondence to: Professor Qi Liu, Department of Neurosurgery, The First Affiliated Hospital of Shihezi University, Shihezi University, 107 North Second Road, Shihezi, Xinjiang 832008, P.R. China
E-mail: liuqi801020@163.com

Key words: astragaloside IV, pituitary tumor, TUBB4B, STMN1, ERK pathway, apoptosis

Introduction

Pituitary tumors are among the most common intracranial neoplasms, accounting for 10-15% of all intracranial tumors (1). Although most pituitary tumors are benign, they cause complications such as abnormal hormone secretion, visual field defect and headache, which impair the quality of life of patients (2). Current treatment strategies for pituitary tumors include surgical resection, medical therapy and radiotherapy. However, issues such as high recurrence rate, drug resistance and side effects persist (3-5). Therefore, exploring novel molecular targeted therapies for pituitary tumors is clinically important.

Astragaloside IV (AS-IV) is among the primary active components of *Astragalus membranaceus*, a traditional Chinese herb (6). AS-IV has been confirmed to possess pharmacological activity, including anti-inflammatory, antioxidant, immunomodulatory and antitumor effects (7). AS-IV provides significant antitumor effects in various tumor models, such as lung (8), liver (9) and breast cancer (10). However, whether AS-IV inhibits pituitary tumors and the underlying molecular mechanism remain unclear. Tubulin β-4B isotype (TUBB4B) is a key member of the tubulin family and is involved in critical biological processes such as cell mitosis (11,12), cytoskeleton formation (13) and intracellular transport (14). TUBB4B is abnormally expressed in non-small cell lung cancer, Behçet's uveitis, and colorectal cancer and is associated with tumor proliferation, invasion and poor prognosis (15-17). In addition, stathmin 1 (STMN1), a microtubule-destabilizing protein, regulates cell cycle progression by modulating microtubule dynamics (18). Its expression is enhanced in triple-negative breast cancer, hepatic fibrosis, and esophageal cancer and is often associated with the activation of the

ERK/MAPK signaling pathway (19). U0126 is an inhibitor of the ERK/MAPK pathway and can suppress ERK pathway activation by inhibiting the activity and phosphorylation of MEK1/2 (20).

The present study aimed to investigate the effects of AS-IV on the proliferation and apoptosis of pituitary tumor cells and explore its antitumor mechanism by targeting TUBB4B to regulate the STMN1/ERK signaling pathway. Through cell experiments, transcriptome sequencing, molecular and dynamics simulation and nude mouse xenograft models, the present study aimed to verify the key role of the AS-IV-regulated TUBB4B-STMN1-ERK axis in driving the development and progression of pituitary tumors, which may provide a novel theoretical basis and potential strategy for targeted therapy of pituitary tumors.

Materials and methods

Materials. The suppliers for all materials are provided in Table I.

Clinical samples. A total of three human pituitary tumor specimens were collected (November 2024 to June 2025) during neurosurgery at the First Affiliated Hospital of Shihezi University, Shihezi, China. The present study was approved by the Scientific and Technological Ethics Committee of the First Affiliated Hospital of Shihezi University (approval no. KJ2024-476-01). Patients with pituitary tumors confirmed by preoperative computed tomography and postoperative pathology were included Exclusion criteria were as follows: Patients with incomplete clinical data; patients who undergone radiotherapy or chemotherapy prior to surgery; samples with poor tissue preservation or insufficient RNA/protein quality. All patients signed a written informed consent form. Patient information is summarized in Table II.

Cell culture. Rat pituitary tumor cell lines (GH3 and MMQ) were obtained from Wuhan Procell Biotechnology Co., Ltd. Both GH3 and MMQ cells were cultured in a GH3-specific complete medium (82.5% Ham's F-12K medium, 15% horse serum, 2.5% FBS and 1% penicillin-streptomycin) in a sterile, humidified incubator at 37˚C with 95% air and 5% CO_2. GH3 cells grew in a loosely adherent manner, while MMQ cells grew in suspension. When confluency reached 70-80%, the cells were passaged at a ratio of 1:3 to maintain exponential growth.

Sequencing and bioinformatics analysis. AS-IV was purchased from MedChemExpress (purity, 99.93%) and dissolved in DMSO according to the manufacturer's instructions. GH3 cells were divided into the AS-IV treatment group (n=6) and DMSO-treated negative control group (NC, n=3). Transcriptomics sequencing was performed at Hangzhou Lianchuan Biotechnology Co., Ltd. RNA was isolated using TRIzol (Invitrogen; Thermo Fisher Scientific, Inc.). The total RNA was quantified and quality-controlled using a NanoDrop ND-1000 (NanoDrop). rRNA was removed using the Epicentre Ribo-Zero Gold Kit (Illumina, Inc.), and cDNA was synthesized from the fragmented RNA using reverse transcriptase (Invitrogen SuperScript™ II Reverse Transcriptase, cat. no. 1896649). Then, *E. coli* DNA polymerase I (NEB, cat. no. m0209) and RNase H (NEB, cat. no. m0297) were used for double-strand synthesis to convert the composite double-stranded RNA-DNA hybrid into double-stranded DNA. The double-stranded DNA was digested with UDG (NEB, cat. no. m0280), followed by PCR (pre-denaturation at 95˚C for 3 min; 8 cycles of denaturation at 98˚C for 15 sec each; annealing at 60˚C for 15 sec; extension at 72˚C for 30 sec, followed by a final extension at 72˚C for 5 min) to generate a library consisting of fragments ranging from 300±50 bp. Finally, the library was sequenced using Illumina Novaseq™ 6000 (LC Bio Technology Co., Ltd.) in a paired-end (PE150) sequencing mode. The library concentration was measured using a Qubit fluorometer (Thermo Fisher Scientific, Inc.) and a High Sensitivity DNA Chip on a Bioanalyzer 2100 (Agilent Technologies), with the final loading concentration adjusted to 2 nM for sequencing.

Low-quality sequences in the raw sequencing data were filtered out via Cutadapt (v1.9; cutadapt.readthedocs.io/). The processed data were used for transcriptome assembly and quantitative analysis. Differentially expressed genes (DEGs) were screened with the limma package (v3.5x; bioinf.wehi.edu.au/limma/) in R (v4.2.1; r-project.org/) with the threshold defined as fold-change (FC) ≥2 or ≤0.5 and q-value <0.05 ($|\log_2 FC| \geq 1$ and $q<0.05$). Gene Ontology (GO) enrichment analysis (geneontology.org/), Gene Set Enrichment Analysis (GSEA; gsea-msigdb.org/), Kyoto Encyclopedia of Genes and Genomes (KEGG) pathway enrichment (kegg.jp/) and protein-protein interaction (PPI) analysis (string-db.org/) were performed using WebGestalt (webgestalt.org/). Partial bioinformatics data were obtained from the Gene Expression Omnibus (GEO) database (accession no. GSE136781; ncbi.nlm.nih.gov/geo/query/acc.cgi?acc=GSE136781) and the STRING database (cn.string-db.org; TUBB4B and STMN1).

Lentivirus-mediated TUBB4B overexpression (OE) and knockdown (KD). The lentiviral vectors used for OE included LV5(EF-1α/GFP&Puro)-TUBB4B (OE-TUBB4B) and LV5 (EF-1α/GFP&Puro)-NC (OE-shNC; both $1x10^9$ TU/ml). The lentiviral vectors used for knockdown LV3-GFP&Puro-TUBB4B-141 (KD1-TUBB4B), LV3-GFP&Puro-TUBB4B-199 (KD2-TUBB4B) and LV3-GFP&Puro-NC (KD-shNC; all $1x10^8$ TU/ml) and polybrene were purchased from Suzhou GenePharma Co., Ltd. The sequences of lentiviral vectors are listed in Table III. The lentiviral packaging system used in this study is a third-generation system. Lentiviral particles were prepared in 293T cells (purchased from GenePharma). For transfection, 10 μg of lentiviral transfer plasmids (expressing TUBB4B or shRNA) were mixed with the packaging plasmids pGag/Pol, pRev, and pVSV-G in a 4:2:2:1 ratio and transfected using Lipofectamine 3000 (Thermo Fisher Scientific, Inc.) at 37˚C for 48 h. After transfection, the supernatant containing lentiviral particles was collected, filtered through a 0.45 μm filter, and concentrated by ultracentrifugation. The viral titer was determined by qPCR and expressed in TU/ml.

GH3/MMQ cells were seeded into 6-well plates at a density of $2x10^5$ cells/well. When cell confluency reached 70%, lentiviral vectors and polybrene were added to 6-well plates containing complete medium (MOI for the GH3 cell

Table I. Suppliers of materials.

Name	Supplier	Cat. no.
GH3 complete medium	Boster Biological Technology	ZYPYG0264
Ham's F-12K	Thermo Fisher Scientific, Inc.	21127030
Horse serum	Thermo Fisher Scientific, Inc.	16050122
Puromycin	MCE	HY-K1057
Fluorescence microscope	Nikon Corporation	ECLIPSE Ts2R
Total RNA kit I	Omega Bio-Tek, Inc.	R6834-01
NanoDrop One	Thermo Fisher Scientific, Inc.	840-317400
cDNA Synthesis kit	Thermo Fisher Scientific, Inc.	K1622
UltraSYBR Mixture PCR	Cwbio	CW0957H
Gentier 96R RT-qPCR	Xi'an Tianlong Science and Technology Co., Ltd.	TL22R221038785
BALB-c nude mice	Hunan SJA Laboratory Animal Co., Ltd.	Not applicable
Paraformaldehyde	Biosharp Life Sciences	BL539A
Triton X-100	Beijing Solarbio Science & Technology Co., Ltd.	T8200
TUNEL	Beyotime Biotechnology	C1086
DAPI	Beyotime Biotechnology	C1005
EdU Imaging kit	APeXBIO	K1075
Crystal violet	Beijing Solarbio Science & Technology Co., Ltd.	G1062
Annexin V-PE/7-AAD	BD Biosciences	BD559763
NovoCyte	ACEA Biosciences, Inc.	None
RIPA	Beyotime Biotechnology	P0013B
NP-40 lysis buffer	Beijing Solarbio Science & Technology Co., Ltd.	N8032
TBS	Wuhan Servicebio Technology Co., Ltd.	G0001
Goat anti-rabbit IgG (H+L) secondary antibody, HRP	Thermo Fisher Scientific, Inc.	C31460100
Goat anti-Mouse IgG (H+L) secondary antibody, HRP	Thermo Fisher Scientific, Inc.	31430
TUBB4B antibody	Boster Biological Technology	BM4264
PCNA antibody	Boster Biological Technology	BM3888
Bcl-2 antibody	Abmart Pharmaceutical Technology Co., Ltd.	T40056
Bax antibody	Abmart Pharmaceutical Technology Co., Ltd.	T40051
Pro-caspase3 antibody	Boster Biological Technology	M00334-9
Cleaved caspase3 antibody	Abmart Pharmaceutical Technology Co., Ltd.	TA7022
Total PARP antibody	Abmart Pharmaceutical Technology Co., Ltd.	P79881
Cleaved PARP antibody	Abmart Pharmaceutical Technology Co., Ltd.	T55035
STMN1 antibody	Abmart Pharmaceutical Technology Co., Ltd.	PA4263
p-STMN1 antibody	Abmart Pharmaceutical Technology Co., Ltd.	TP56510
cPLA2 antibody	Abmart Pharmaceutical Technology Co., Ltd.	PA3288
p-cPLA2 antibody	Abmart Pharmaceutical Technology Co., Ltd.	PA3287
CCND1 antibody	Boster Biological Technology	PB0403
ERK antibody	Abmart Pharmaceutical Technology Co., Ltd.	T40071
p-ERK antibody	Abmart Pharmaceutical Technology Co., Ltd.	T40072
JNK antibody	Abmart Pharmaceutical Technology Co., Ltd.	T40073
p-JNK antibody	Abmart Pharmaceutical Technology Co., Ltd.	T40074
GAPDH antibody	Boster Biological Technology	A00227
Tween-20	Beyotime Biotechnology	ST825
BSA	BioFroxx; neoFroxx	4240GR100
Rapid blocking solution	Epizyme	PS108P
Stripping buffer	Cwbio	CW0056M
ECL solution	Biosharp Lifesciences	BL520A/B
Goat anti-rabbit IgG (H+L) Secondary antibody, Alexa Fluor-488	Wuhan Sanying Biotechnology	SA00013-2
Phalloidin	Suzhou UYiLandi Biotechnology Co., Ltd.	YP0052

Table I. Continued.

Name	Supplier	Cat. no.
Hoechst-33342	MCE	HY-15559A
HRP-conjugated goat anti-mouse/rabbit IgG	Wuhan Servicebio Technology Co., Ltd.	TBAG0036
Hematoxylin	Wuhan Servicebio Technology Co., Ltd.	G1004
Eosin	Wuhan Servicebio Technology Co., Ltd.	G1001
Citric acid	Wuhan Servicebio Technology Co., Ltd.	G1201
Endogenous peroxidase blocking buffer	Beyotime Biotechnology	P0100A
IHC secondary antibody	Wuhan Servicebio Technology Co., Ltd.	G1303
DAB	Wuhan Servicebio Technology Co., Ltd.	G1212
U0126	MCE	HY-12031A

MCE, MedChemExpress; RT-q, reverse transcription-quantitative; TUBB4B, tubulin β4B class IVb; STMN1, stathmin 1; p-, phospho-; cPLA2, cytosolic phospholipase A2; CCND1, cyclin D1; IHC, immunohistochemistry.

Table II. Patient information.

No.	Age, years	Sex	Knosp grade	Subtype of Pituitary Tumors
1	46	Male	IV	GH
2	53	Male	IV	GH
3	37	Female	II	P

GH, growth hormone-secreting pituitary adenoma; P, prolactin.

Table III. Lentivirus-mediated RNA sequences for stable transfection.

Name	Sequence, 5'→3'	Note
Vector	TAATATCCCTCTTTAAGTGT	Non-targeting sequence inserted into the lentiviral backbone JLVO-CAG-GFP-Apuro (9771 bp)
OE-TUBB4B	NM_199094.3 (1338 bp)	Full-length coding sequence of TUBB4B
shNC	TTCTCCGAACGTGTCACGT	Scrambled non-targeting shRNA
KD1-TUBB4B	GCGACGAGCATGGCATTGATC	shRNA targeting TUBB4B
KD2-TUBB4B	GGAGCGCATCAACGTGTACTA	shRNA targeting TUBB4B

OE, overexpression; TUBB4B, tubulin β4B class IVb; sh, short hairpin; NC, negative control; KD, knockdown.

line was ~50, and for the MMQ cell line, ~100) and allow transfection to proceed for 24-48 h at 37˚C and 5% CO_2. After 72 h, the cells were selected with 1 μg/ml puromycin for 48 h at 37˚C and 5% CO_2 to establish stably transfected cell lines, and 1 μg/ml puromycin was used to maintain the continued culture of stably transfected cells. The transfection efficiency of the stably transfected cell lines was verified by reverse transcription-quantitative (RT-q)PCR and western blotting. Cells stably transfected for up to 2 weeks were used for subsequent experiments.

RT-qPCR. Total RNA was extracted from the GH3/MMQ cells using Total RNA kit I, and the RNA concentration was quantified with a NanoDrop One device. cDNA was synthesized via one-step RT using the RevertAid First Strand cDNA Synthesis kit following the manufacturer's instructions. Target cDNA fragments were amplified and detected using UltraSYBR Mixture PCR reagents on a Gentier 96R RT-qPCR system (Xi'an Tianlong Technology Co., Ltd.) according to the manufacturer's instructions. The thermocycling conditions were as follows: initial denaturation at 95˚C for 10 min, followed by 40 cycles of 95˚C for 15 sec and 60˚C for 60 sec). GAPDH was adopted as the internal reference to normalize the relative expression of target mRNAs, and the $2^{-\Delta\Delta Cq}$ method (21) was employed for quantitative analysis of relative nucleic acid expression. All primer sequences are listed in Table IV.

Table IV. Primer sequences for reverse transcription-quantitative PCR.

Gene	Forward primer, 5'→3'	Reverse primer, 5'→3'
TUBB4B	ATTGATCCCACTGGCACGTA	TCACAACGTCCAACACCGAG
GAPDH	GACATGCCGCCTGGAGAAAC	AGCCCAGGATGCCCTTTAGT
CCNA1	TGAACAGGGGGACAGAGACA	GAGTCAACCAGCATTGGGGA
CCNB1	ATTGCAGCTGGGGCTTTTTG	AGAGATTCCTCCGTGTGGGA
CCND1	CAAGTGTGACCCGGACTGC	GCAAGCCAGACCAGCTTCTT
CCNE1	CGTTTAAGCCCCCTGACCAT	CACTTCTCCCGTGTCGTTGA
CDK1	TATCCCTCCTGGCCAGTTCA	GGTACCACAGCGTCACTACC
CDK2	AAATCCGGCTCGACACTGAG	TCCAGCAGCTTGACGATGTT
CDK4	GATGCGCCAGTTTCTAAGCG	AGGGCCATCTGGTAGCTGTA
CDK6	GTGGACCTCTGGAGTGTTGG	CCACGTCTGAACTTCCACGA

TUBB4B, tubulin β4B class IVb; CCN, cyclin.

BALB/c nude mouse model establishment. The animal experiments were approved by the Bioethics Committee of Shihezi University, Shihezi, China (approval no. A2024-353). Thirty female BALB/c nude mice (age, 3-4 weeks old; weight, 15-18 g at the start of the study) were purchased from Helilai Co., Ltd. and housed in a specific pathogen-free environment (temperature, 24±2˚C; humidity, 50-60%; 12 h light/dark cycle) with *ad libitum* access to sterilized food and water. At the start of the experiment, each nude mouse was injected with $2x10^6$ GH3 cells suspended in 100 μl PBS into the left axilla. Mice in the Vector + AS-IV, OE-TUBB4B + AS-IV and KD2-TUBB4B+AS-IV) with n=5 per subgroup, were intraperitoneally injected with AS-IV at a half-maximal inhibitory concentration (IC_{50}) dose of 10-20 mg/kg daily, whereas the mice in the control group, consisting of three subgroups (Vector, OE-TUBB4B, and KD2-TUBB4B) with n=5 per subgroup (total n=15),were intraperitoneally injected with the same volume of normal saline daily. Humane endpoints, including tumor diameter exceeding 15 mm, significant weight loss, and visible signs of tumor ulceration or infection. The body weight and the length/width of the subcutaneous tumors were measured every 3 days. The mice were euthanized by cervical dislocation following 21 days of continuous feeding; death was confirmed by the absence of a heartbeat, cessation of breathing and fixed, dilated pupils. Tumor samples were weighed and stored for further analysis.

Cell viability assay. GH3/MMQ cells were seeded into 96-well plates at a density of $8x10^3$ cells/well and cultured in a 37˚C for 24 h. The cells were cultured in 100 μl GH3 complete medium containing AS-IV at (0 to 140 μM in a 37˚C, 5% CO_2 incubator for 0-72 h. At 0, 24, 48, and 72 h, 10 μl Cell Counting Kit 8 (CCK-8) reagent and 90 μl F12K medium were added to each well, followed by incubation for 2 h. The optical density at 450 nm was measured using a microplate reader.

To investigate the mechanism of TUBB4B, GH3 cells were transduced with lentivirus to establish OE-TUBB4B and Vector stable cell lines. Following the manufacturer's instructions, the cells were treated with 60 nM U0126 (a MEK/ERK pathway inhibitor) at 37˚C with 5% CO_2 for 48 h, after which cell viability was assessed using the CCK-8 assay.

TUNEL assay for apoptosis detection. GH3 cells were seeded into 24-well plates at a density of $1x10^5$ cells/well. After incubating for 24 h at 37˚C and 5% CO_2, the GH3 complete medium was replaced with GH3 complete medium containing AS-IV ranging from 0 to 160 μM, and the cells were cultured at a 37˚C for 48 h. The cells were washed three times with PBS and 500 μl 4% paraformaldehyde was added for 15 min at room temperature. The cells were permeabilized with 0.4% Triton X-100 for 10 min at room temperature. A TUNEL apoptosis detection kit was used according to the manufacturer's instructions. The nuclei were stained at room temperature in the dark for 20 min with DAPI at a final concentration of 1 μg/ml. Finally, the slides were mounted with 50% glycerol in PBS, cells were observed using a fluorescence microscope and the number of TUNEL-positive cells was counted using ImageJ software (v1.54p; National Institutes of Health).

EdU assay for proliferation detection. GH3 cells were seeded into 24-well plates at a density of $1x10^5$ cells/well. After incubating for 24 h at 37˚C, the medium was replaced with a GH3 complete medium containing 112.3 μM AS-IV, and the cells were cultured at 37˚C for 48 h. An EdU Imaging kit was used according to the manufacturer's instructions to stain nuclei in the S phase. Nuclei were stained at room temperature in the dark for 20 min with DAPI at a final concentration of 1 μg/ml. The results were observed using a fluorescence microscope, and the number of EdU-positive cells was counted using ImageJ software.

Colony formation assay. GH3 cells were seeded into 6-well plates at a density of 500 cells/well. The medium was changed every 3 days, and the cells were cultured at 37˚C for 12-15 days. At room temperature, a total of 1 ml 4% paraformaldehyde was added to each well to fix the cells for 15 min, followed by staining with 0.1% crystal violet for 15 min. Excess crystal violet was removed by washing with water. Colonies were defined as clusters containing >50 cells. Images were captured using a light microscope, and the number of colonies was counted using ImageJ software.

Flow cytometry for apoptosis and cell cycle detection. The cells from the Vector, Vector + AS-IV, OE-TUBB4B+AS-IV, and KD2-TUBB4B+AS-IV groups were collected, resuspended in precooled PBS at a density of $1x10^6$ cells/ml and centrifuged at 400 x g and 4˚C for 5 min. The supernatant was discarded, and the cells were resuspended in 200 μl PBS. A total of 5 μl Annexin V-PE and 5 μl 7-AAD apoptosis detection reagents were added and incubated at 4˚C in the dark for 30 min. Following addition of 300 μl PBS, detection was performed using an ACEA NovoCyte (Agilent Technologies) flow cytometer. The total number of cells undergoing early and late apoptosis was calculated, using NovoExpress software (v1.5.6; Agilent Technologies).

Western blotting. GH3/MMQ cells and tumors from the nude mice were collected. Protein samples were extracted using RIPA lysis buffer, and the protein concentration was quantified with an enhanced Bicinchoninic Acid Protein Assay kit. 50 μg proteins were loaded into each lane; after separation by 10% SDS-PAGE and transferred to a 0.45 μm PVDF membrane. The PVDF membrane was blocked with 5% (w/v) non-fat dry milk in Tris-buffered saline containing 0.1% Tween-20 at room temperature for 1 h, incubated with the primary antibody at 4˚C overnight and incubated with the corresponding horseradish peroxidase-conjugated secondary antibody at room temperature for 1 h. Western blots were visualized using ECL reagent, and analyzed using ImageJ software. Antibodies were as follows: TUBB4B 1:1,000; PCNA 1:2,000; Bcl-2 1:1,000; Bax 1:1,000; pro-caspase-3 1:1,000; cleaved-caspase-3 1:1,000; T-PARP 1:1,000; cleaved-PARP 1:1,000; STMN1 1:500; p-STMN1 1:1,000; cPLA2 1:1,000; p-cPLA2 1:500; CCND1 1:1,000; ERK 1:1,000; p-ERK 1:1,000; JNK (1:1,000); p-JNK 1:1,000; GAPDH 1:20,000; Goat anti-rabbit 1:20,000; Goat anti-mouse 1:20,000.)

Hematoxylin and eosin (H&E) and immunohistochemical (IHC) staining. Human pituitary and mouse tumor specimens were fixed with a 4% paraformaldehyde solution at room temperature for 24 h, followed by paraffin embedding and serial sectioning (thickness, 4 μm). For H&E staining, the sections were rehydrated and stained with hematoxylin solution (0.5%) for 3-5 min, followed by eosin Y solution (0.5%) for 15-20 sec at room temperature. For IHC staining, the sections were rehydrated and antigen retrieval was performed in high-temperature citric acid solution at 160˚C for 10 min and washed with PBS. Sections were blocked with 3% H_2O_2 at room temperature for 10 min, followed by blocking with PBS containing 5% BSA at room temperature for 30 min. Primary antibodies against TUBB4B (1:100), PCNA (1:100), Bcl-2 (1:200), Bax (1:100) and cleaved-caspase-3 (1:200) were added at 4˚C in the dark overnight. The sections were incubated with a universal secondary antibody (HRP-conjugated goat anti-mouse/rabbit IgG, Servicebio; catalog No. TBAG0036) at a dilution of 1:200 at room temperature for 1 h. DAB chromogen was added for 20 min. For nuclear counterstaining, the sections were stained with hematoxylin at room temperature for 1-2 min. The sections were observed and photographed using a light microscope (Olympus BX53).

Immunofluorescence staining. GH3 cells stably transfected with lentiviruses were seeded into confocal dishes at a density of $1x10^5$ cells/dish. Subsequently, cells in the Vector, OE-TUBB4B+AS-IV, and KD2-TUBB4B+AS-IV groups were treated with AS-IV at a concentration of 112.3 μM at 37˚C for 48 h, fixed with 4% paraformaldehyde at room temperature for 15 min, and permeabilized with 0.4% Triton X-100 at room temperature for 10 min. The cells were stained with phalloidin at room temperature in the dark for 20 min, placed in blocking solution for 30 min, incubated with TUBB4B primary antibody (1:100) at 4˚C overnight, and then incubated with fluorescent secondary antibody [goat anti-rabbit IgG (H+L), conjugated with Alexa Fluor-488; 1:200] at room temperature for 1 h. The nuclei were stained with Hoechst 33342 (10 μg/ml) for 20 min at room temperature. Finally, images were captured using a confocal microscope.

Molecular docking and dynamics simulation. AutoDockTools software (v1.5.7; http://autodock.scripps.edu/) was used to preprocess the conformations of AS-IV and TUBB4B and appropriate docking sites were selected. AutoDock Vina software (v1.1.2; vina.scripps.edu/) was used to select the optimal molecular docking conformation. PyMOL software (v2.3.0; pymol.org/) and LigPlot+ software (v2.2.8; ebi.ac.uk/thornton-srv/software/LigPlus/) were used for analysis and visualization.

Amber24 software (ambermd.org/) was used for molecular dynamics simulation purposes, with the ff19SB force field and Optimal Point Charge (OPC) water model selected. The AS-IV-TUBB4B complex was placed in a cubic water box. The cutoff distance for electrostatic and van der Waals interactions was set to 1.0 nm, the time step was 2 femtosecond (fs) and the particle-mesh Ewald method (22) used for long-range correction of electrostatic interactions. Energy minimization was performed, followed by 200 ps Microcanonical ensemble (NVE) equilibrium dynamics and 100 ps number of particles, pressure and temperature) equilibrium dynamics. The V-rescale method was used for temperature coupling of the thermal bath system (23) and the Parrinello-Rahman method was used for pressure control (24). Finally, 100 nsec molecular dynamics sampling was performed. Indicators such as root mean square fluctuation (RMSF), root mean square deviation (RMSD), radius of gyration (Rg) and solvent-accessible surface area (SASA) were calculated using Amber modules (AmberTools24; https://ambermd.org), Cpptraj (v5.1.0; github.com/Amber-MD/cpptraj) and Python scripts (v3.10; https://www.python.org).

Cell thermal shift assay (CETSA). GH3 cells in the logarithmic growth phase were treated with 112.3 μM AS-IV at 37˚C for 24 h in the shNC, OE-TUBB4B and KD2-TUBB4B groups. Following trypsin digestion, the cells were resuspended and aliquoted at $1x10^6$ cells/well into eight EP tubes. The tubes were heated for 10 min across a temperature gradient (35-70˚C). NP-40 lysis buffer was added and the sample was centrifuged at 4˚C, 20,000 x g for 20 min. The protein supernatant was collected. The TUBB4B protein expression was detected via western blot analysis as aforementioned. Melting curves were plotted by analyzing changes in TUBB4B solubility or abundance at different temperatures.

Statistical analysis. Statistical analysis was performed using GraphPad Prism 10 (Dotmatics). All experiments were

repeated at least three times, and all data are expressed as the mean ± SD. One- or two-way ANOVA followed by Dunnett's t test was used for comparisons. $P<0.05$ was considered to indicate a statistically significant difference.

Results

AS-IV inhibits proliferation and promotes apoptosis of GH3/MMQ cells in a concentration- and time-dependent manner. CCK-8 assay demonstrated that AS-IV significantly inhibited the activity of GH3 and MMQ cells in a concentration- and time-dependent manner (Fig. 1D-K). The chemical structure of AS-IV is shown in Fig. 1A. The IC_{50} values detected after 48 h AS-IV treatment in GH3 and MMQ cells were 112.3 and 247.7 μM, respectively (Fig. 1B and C). To ensure consistency in subsequent experiments, 48 h was selected as the treatment duration and IC_{50} values were used as the drug concentration for AS-IV intervention.

TUNEL assay was performed to confirm that AS-IV promotes apoptosis in GH3 cells in a concentration-dependent manner (Fig. 1L). The apoptosis rate of the GH3 cells treated with 160 μM AS-IV was significantly greater than that of the control cells (Fig. 1M). Western blot analysis of apoptosis-associated proteins (Fig. S1A) revealed that the expression of cleaved-PARP (Fig. S1C) significantly increased in AS-IV-treated cells. The expression of the 113 kDa total PARP isoform decreased but that of the 89 kDa form increased, however there was no significant difference in total protein levels (Fig. S1B and C). Western blotting revealed that pro-caspase3 protein levels remained largely unchanged in AS-IV-treated cells, whereas the relative expression of cleaved-caspase3 protein (Fig. S1D-F) was significantly elevated. Transmission electron microscopy revealed increased numbers of vesicles, apoptotic bodies, fragmented mitochondrial tubular networks and loss of mitochondrial cristae fusion in AS-IV-treated cells (Fig. S1G). These findings confirmed that AS-IV induces pituitary tumor cell apoptosis.

Transcriptome sequencing reveals significant downregulation of TUBB4B in AS-IV-treated GH3 cells and high expression of TUBB4B in pituitary tumors. To explore the key signals and related pathways underlying the AS-IV-mediated inhibition of GH3 cell proliferation, single-cell sequencing of AS-IV-treated GH3 cells was performed. Compared with the NC group, 931 up- and 829 downregulated DEGs were identified (Fig. 2A and B). GO enrichment analysis in the biological process category (Fig. 2C) revealed that the functions of the DEGs were enriched in 'DNA replication' and 'cell cycle'. A heatmap of the transcriptomic DEGs (Fig. 2D) revealed that the tubulin family (which synthesizes the cytoskeleton) (25), especially TUBB, was significantly downregulated in the AS-IV group. GSEA revealed that genes were significantly downregulated in 'mitotic cell cycle', 'cyclin-dependent protein kinase holoenzyme complex', 'double-stranded RNA binding' and 'structural constituent of cytoskeleton' (Fig. 2E-H). As these enriched gene sets are associated with tubulin-associated functions, it was hypothesized that there was a potential link between cytoskeletal organization and RNA binding, with TUBB4B possibly serving as a bridging molecule. To explore this hypothesis, we selected the gene lists of 'double-stranded RNA binding' and 'structural constituent of cytoskeleton' to construct a Venn diagram (Fig. 2I), which revealed that TUBB4B was present in the intersection. It was hypothesized that TUBB4B may be a key gene mediating AS-IV-induced inhibition of pituitary tumor proliferation and promotion of apoptosis. GEO data demonstrated that TUBB4B expression in pituitary tumor tissues was significantly higher than that in normal pituitary tissue (Fig. 2J), which was consistent with the IHC staining results of pituitary tumor tissue from patients (Fig. 2K). These results confirm that TUBB4B is highly expressed in pituitary tumors.

TUBB4B promotes proliferation and inhibits apoptosis in pituitary tumor cells. Stably transfected cell lines with lentivirus-mediated OE-TUBB4B or knockdown were established (Fig. 3A). The transfection efficiency was verified by RT-qPCR and western blotting (Fig. 3B, C and E-G). The results confirmed the successful establishment of stably transfected cell lines. In both cell lines, the knockdown efficiency of KD2-TUBB4B was greater than that of KD1-TUBB4B; therefore, the KD2-TUBB4B stable cell line was selected for subsequent experiments.

Cell viability was assessed with the CCK-8 assay. In both cell lines, viability in the OE-TUBB4B group was greater than that in the shNC group, which was significantly greater than that in the KD2-TUBB4B group (Fig. 3D and H). EdU assays revealed that the number of proliferating GH3 cells (in the S phase of DNA synthesis; red fluorescence) was highest in the OE-TUBB4B group and lowest in the KD2-TUBB4B group (Fig. 3I and K). Colony formation assay (Fig. 3J and L) revealed that the number of colonies in the OE-TUBB4B group was significantly greater than that in the shNC group, which was greater than that in the KD2-TUBB4B group. Flow cytometry confirmed that OE-TUBB4B decreased the proportion of apoptotic cells, whereas KD-TUBB4B increased the percentage of apoptotic cells in both cell lines (Fig. 3M and O). Western blotting was used to verify the expression of proliferation-associated protein (PCNA) and apoptosis-related proteins (Bcl-2, Bax, pro-caspase-3 and cleaved-caspase-3) in both cell lines (Fig. 3N and P-T). OE-TUBB4B cells had increased expression of PCNA and antiapoptotic protein (Bcl-2) and decreased expression of proapoptotic proteins (Bax and cleaved-caspase-3); in KD2-TUBB4B cells, decreased expression of PCNA and Bcl-2 was observed, along with increased expression of Bax and cleaved-caspase-3. Cells in the OE-TUBB4B group exhibited increased expression of PCNA and Bcl-2 and decreased expression of Bax and cleaved caspase-3; in contrast, cells in the KD2-TUBB4B group exhibited decreased expression of PCNA and Bcl-2, and increased expression of Bax and cleaved caspase-3, confirming the regulatory role of TUBB4B. In summary, TUBB4B promotes the proliferation and inhibits the apoptosis of pituitary tumor cells.

AS-IV exerts an inhibitory effect on pituitary tumors by targeting TUBB4B. To verify that AS-IV inhibits pituitary tumors by targeting TUBB4B, molecular conformations of TUBB4B and AS-IV were generated. The surface electrostatic potential of the TUBB4B protein is shown in Fig. 4A, and molecular docking was performed between AS-IV and

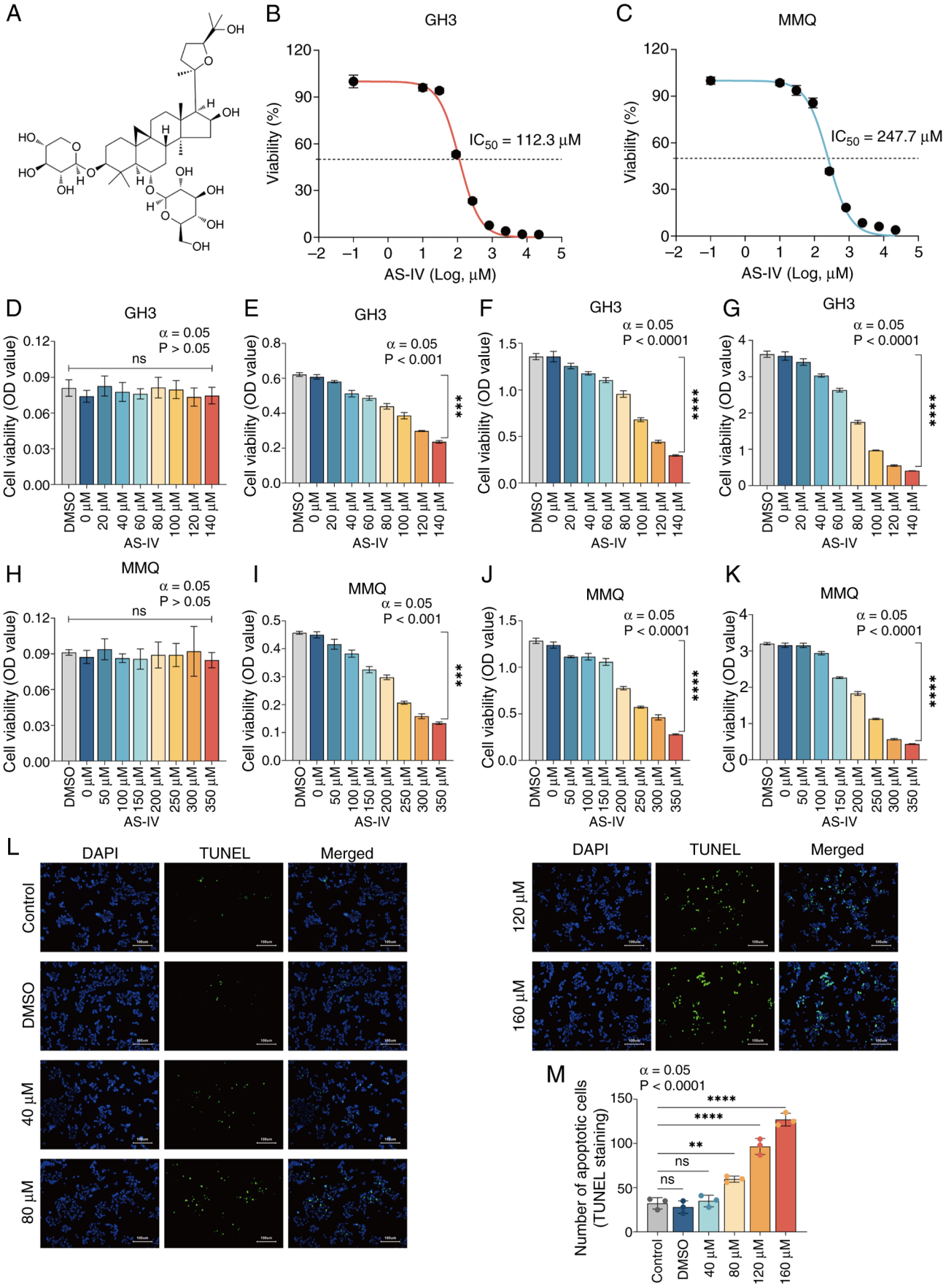

Figure 1. AS-IV inhibits the proliferation and promotes the apoptosis of GH3/MMQ cells in a concentration- and time-dependent manner. (A) Chemical structure of AS-IV. IC_{50} of AS-IV in (B) GH3 and (C) MMQ cells following 48 h treatment. Viability of the GH3 cells treated with 0-140 μM AS-IV at (D) 0, (E) 24, (F) 48 and (G) 72 h. Viability of MMQ-treated cells treated with 0-350 μM AS-IV at (H) 0, (I) 24, (J) 48 and (K) 72 h. (L) TUNEL assay was used to assess the apoptotic effect of AS-IV on GH3. (M) Number of apoptotic cells in each group. ****P<0.0001, ***P<0.001, **P<0.01 vs. control. ns, not significant; AS-IV, astragaloside IV; IC_{50}, half-maximal inhibitory concentration; OD, optical density.

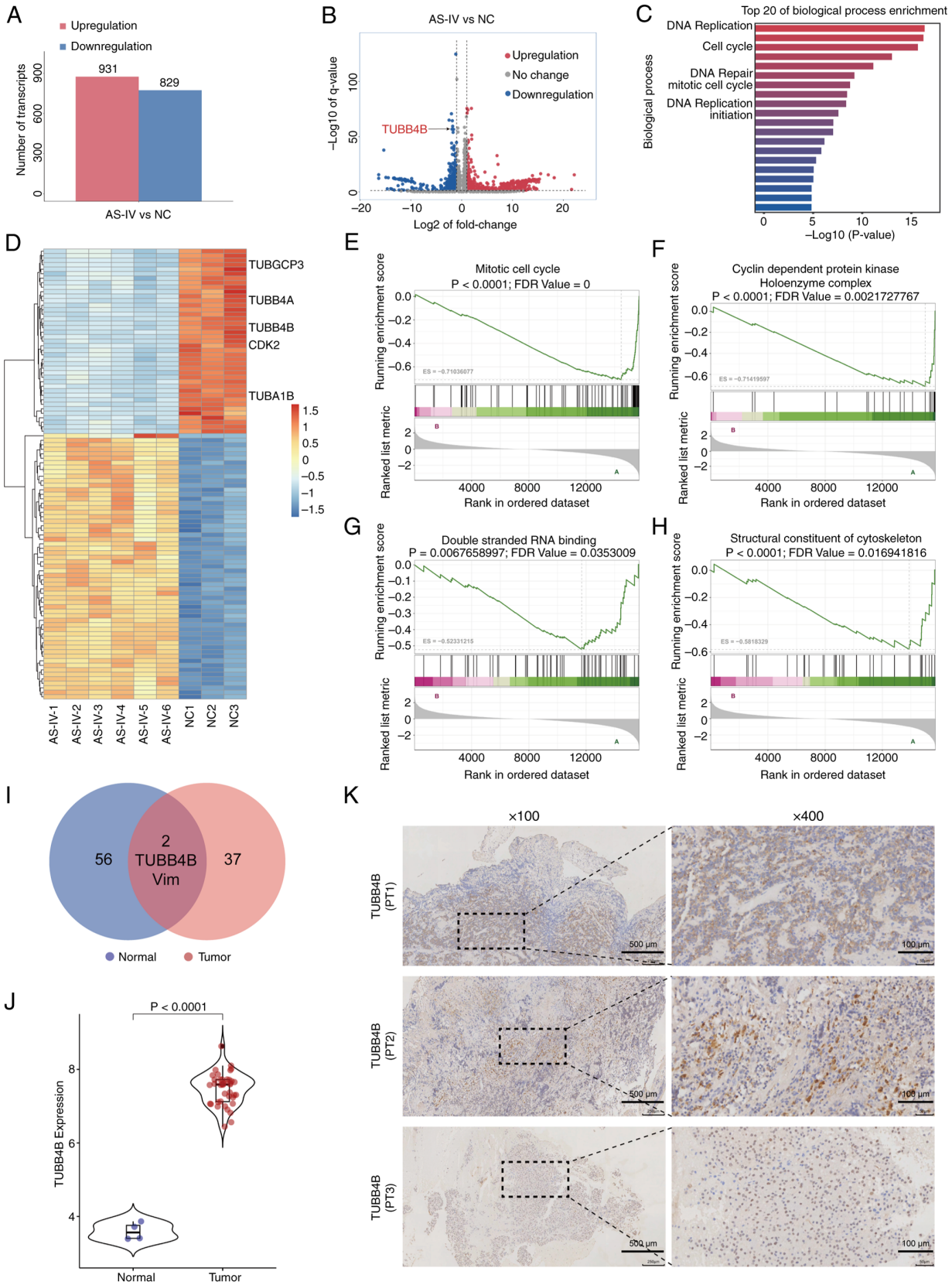

Figure 2. Transcriptomic sequencing reveals that the TUBB4B gene is significantly downregulated in GH3 cells treated with AS-IV and TUBB4B is highly expressed in pituitary tumors. (A) Number of DEGs between the AS-IV and NC group. (B) Volcano plot showing the distribution of DEGs. (C) Gene Ontology enrichment analysis for the biological processes. (D) Heatmap of the expression of significant DEGs. Gene set enrichment analysis demonstrated that down-regulated DEGs were enriched in (E) 'mitotic cell cycle', (F) 'cyclin-dependent protein kinase holoenzyme complex', (G) 'double-stranded RNA binding' and (H) 'structural constituent of cytoskeleton' (ES<-0.5; P<0.05; FDR<0.25). (I) Venn diagram of genes enriched in 'double-stranded RNA binding' and 'structural constituent of cytoskeleton' showing that the TUBB4B gene is at the intersection. (J) Expression of TUBB4B in normal human pituitary glands and pituitary tumors; TUBB4B was highly expressed in pituitary tumors (data from GSE136781, P<0.0001). (K) Immunohistochemical staining of TUBB4B in tissue samples from PTs with pituitary neuroendocrine tumors. TUBB4B, tubulin β4B class IVb; AS-IV, Astragaloside IV; DEG, differentially expressed genes; NC, negative control; ES, enrichment score; FDR, false discovery rate; PT, pituitary tumor; Vim, vimentin.

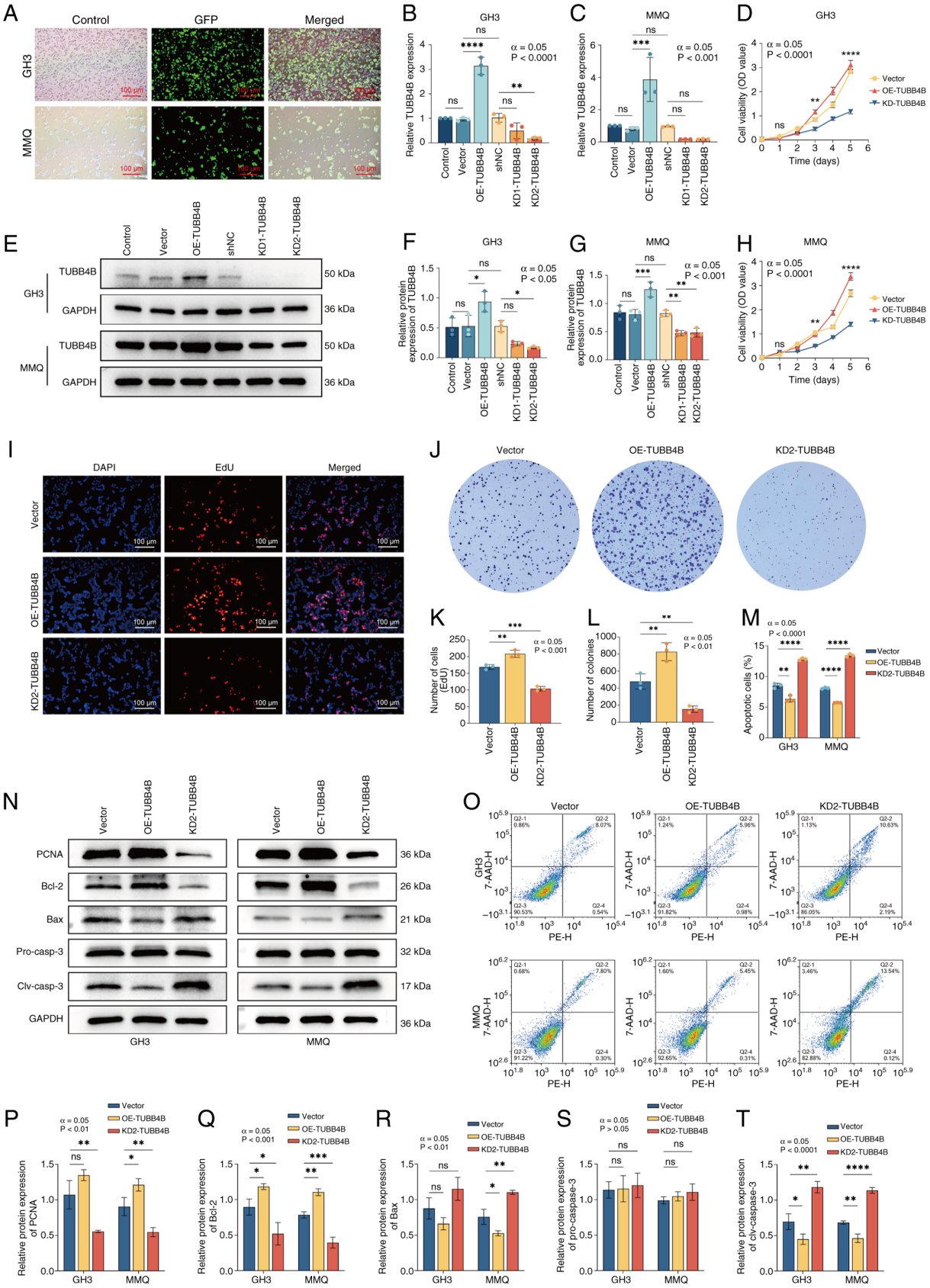

Figure 3. TUBB4B promotes the proliferation and inhibits the apoptosis of pituitary tumor cells. (A) Fluorescence images of the GH3/MMQ cells transfected with lentivirus. Reverse transcription-quantitative PCR was used to assess expression efficiency of TUBB4B in lentivirus-transfected (B) GH3 and (C) MMQ cell lines. (D) Cell Counting Kit-8 assay was used to assess the viability of GH3 cells. (E) Western blotting was used to assess expression efficiency of TUBB4B in lentivirus-transfected (F) GH3 and (G) MMQ cell lines. (H) Cell Counting Kit-8 assay was used to assess the viability of MMQ cells. (I) EdU staining was used to assess the effect of TUBB4B on the proliferation of GH3 cells. (J) Colony formation of GH3 cells. (K) EdU-positive cells. (L) Number of colonies. (M) Number of apoptotic GH3/MMQ cells. (N) Western blot bands (O) Flow cytometry. Western blotting was used to assess protein expression of (P) PCNA, (Q) Bcl-2, (R) Bax, (S) pro-caspase-3 and (T) clv caspase-3 in GH3 and MMQ cell lines. ****P<0.0001, ***P<0.001, **P<0.01, *P<0.05 vs. vector. TUBB4B, tubulin β4B class IVb; OE, overexpression; shNC, short hairpin RNA negative control; KD, knockdown; OD, optical density; clv, cleaved; ns, not significant.

TUBB4B (Fig. 4B). The binding energies of multiple TUBB4B protein conformations with AS-IV indicated a high degree of fit in the binding pocket and a binding energy of -8.2 kcal/mol (Fig. 4C). These findings confirmed that AS-IV and TUBB4B had strong binding activity and bind under natural conditions. On the basis of the molecular docking results, a 100 nsec molecular dynamics simulation was performed on the AS-IV-TUBB4B complex to investigate its binding stability and dynamic behavior. RMSF (Fig. 4D) of the AS-IV-TUBB4B complex fluctuated at residues 56, 80, 175, 277-282 and 427, which may be associated with the function of TUBB4B affected by AS-IV; the RMSD (Fig. 4E) fluctuated in the early stage (0-20 nsec) but stabilized at 20-100 nsec, indicating that the structure of the complex was relatively stable; the Rg value (Fig. 4F) remained stable at ~2.1 nm, indicating that the structure of the complex was compact and the SASA (Fig. 4G) of the entire system was relatively stable. Free energy landscape of the complex demonstrated that the conformation of the AS-IV-TUBB4B complex was stable when the Rg values ranged from 2.07 to 2.09 nm and the RMSD was 0.03-0.17 nm (Fig. 4H).

The present study demonstrated the targeted interaction between AS-IV and TUBB4B by verifying whether TUBB4B regulation directly influences the pharmacological efficacy of AS-IV. Immunofluorescence demonstrated the shNC + AS-IV group exhibited partial cell shrinkage, nuclear condensation and blurred or fragmented cytoskeletal structures (Fig. 4J). In the OE-TUBB4B + AS-IV group, some nuclei were markedly lysed and the cytoskeletal components were fragmented and degraded in the cytoplasm, indicating that OE-TUBB4B enhances the inhibitory effect of AS-IV on pituitary tumors. Conversely, in the KD2-TUBB4B + AS-IV group, although nuclei shrank, the cytoskeletal structure remained intact, suggesting that KD-TUBB4B attenuated the inhibitory effect of AS-IV on pituitary tumors. The present study validated the targeted interaction between AS-IV and the TUBB4B protein via CETSA. TUBB4B protein gradually denatured with increasing temperature (Fig. S2A). In AS-IV-treated cells, the thermal denaturation temperature of the TUBB4B protein increased. Compared with that in the shNC group (Fig. S2B), the melting curve in the OE-TUBB4B group shifted to the right (Fig. S2C), whereas the KD2-TUBB4B group showed the opposite trend (Fig. S2D and E), indicating direct binding of AS-IV to TUBB4B. The present study determined the effect of TUBB4B on AS-IV drug sensitivity via viability assays. In the shNC group, the IC_{50} was 112.8 μM, reflecting baseline sensitivity, whereas in the OE-TUBB4B group, the IC_{50} was 60.4 μM and that in the KD2-TUBB4B group was 292.1 μM (Fig. S2F). The cells overexpressing TUBB4B exhibited increased sensitivity to AS-IV, whereas KD-TUBB4B expression decreased AS-IV sensitivity. Flow cytometry (Fig. 4I and L), EdU assay (Fig. 4K and M) and western blot analysis were performed for both cell lines (Fig. 4N-S). The cells in the OE-TUBB4B + AS-IV group proliferated more slowly and exhibited a higher apoptosis rate than those in the Vector + AS-IV group; in contrast, cells in the KD2-TUBB4B+AS-IV group proliferated more rapidly and exhibited a lower apoptosis rate compared to the Vector + AS-IV group. These results collectively confirmed that OE-TUBB4B enhanced AS-IV efficacy, whereas KD-TUBB4B attenuated it, indicating that TUBB4B modulates cellular sensitivity to AS-IV. These findings collectively demonstrated that AS-IV targeted TUBB4B to exert its inhibitory effect on pituitary tumors.

OE-TUBB4B upregulates STMN1 and activates the ERK pathway. To clarify the mechanism by which TUBB4B affects the proliferation and apoptosis of pituitary tumors, the cell cycle of GH3 cells was analyzed. OE-TUBB4B accelerated the G1-to-S phase transition (Fig. 5A and B). RT-qPCR was used to assess cell cycle-related protein expression (Fig. 5C); expression levels of CCND1, CDK4 and CDK6 were significantly increased in the OE-TUBB4B group, consistent with the KEGG pathway enrichment (Fig. 5D). PPI analysis (Fig. 5E) revealed that the TUBB4B protein interacted with STMN1, which was consistent with the data from the STRING database (Fig. 5F). Therefore, the present study focused on the regulation of the ERK/MAPK pathway by the STMN1 protein.

To verify whether changes in STMN1 expression directly relied on TUBB4B regulation, immunofluorescence colocalization of the TUBB4B and STMN1 protein was performed (Fig. S3A). Upon OE of TUBB4B, the green (TUBB4B) and the red fluorescence signal (STMN1) increased. Following KD of TUBB4B expression, the fluorescence signals of both TUBB4B and STMN1 simultaneously decreased, with a corresponding decrease in colocalization. These results indicate that STMN1 expression was associated with TUBB4B levels and that STMN1 colocalized within the microtubule network. Western blot analysis demonstrated OE-TUBB4B increased expression of the STMN1, p-STMN1, ERK and p-ERK proteins (Fig. S3B), whereas KD-TUBB4B decreased expression (Fig. S3C-F). These findings indicate that STMN1 served as an effector molecule in the TUBB4B downstream pathway and was associated with ERK pathway activation.

CCK-8 assay revealed no significant difference in cell viability between the OE-TUBB4B and the shNC group following U0126 treatment (Fig. 5G). Western blot analysis (Fig. 5H-Q) indicated that OE-TUBB4B led to increased expression of p-STMN1, p-cPLA2, p-ERK and CCND1. Additionally, the expression of total STMN1, cPLA2 and ERK proteins increased, and no significant differences in the levels of the JNK and p-JNK protein were detected. Following U0126 treatment, the STMN1, p-STMN1, cPLA2, p-cPLA2, ERK, p-ERK, CCND1, JNK, and p-JNK protein levels in the Vector + AS-IV group or the OE-TUBB4B+AS-IV group did not significantly change. These findings indicated that the ERK/MAPK pathway is involved in proliferation and that blocking this pathway inhibited positive feedback. These findings also suggest that OE-TUBB4B may promote pituitary tumor proliferation through the activation of positive feedback among downstream proteins.

AS-IV inhibits proliferation and promotes the apoptosis of xenograft tumors in vivo by targeting TUBB4B. To verify the reliability of the *in vitro* cell experiments *in vivo*, a nude mouse subcutaneous xenograft model was established using TUBB4B-regulated GH3 cell lines (Fig. 6A). There was no significant difference in body weight between any groups (Fig. 6B), which was attributed to the benign nature of the GH3 cell line. Compared with the Vector group, both tumor volume and weight were significantly increased

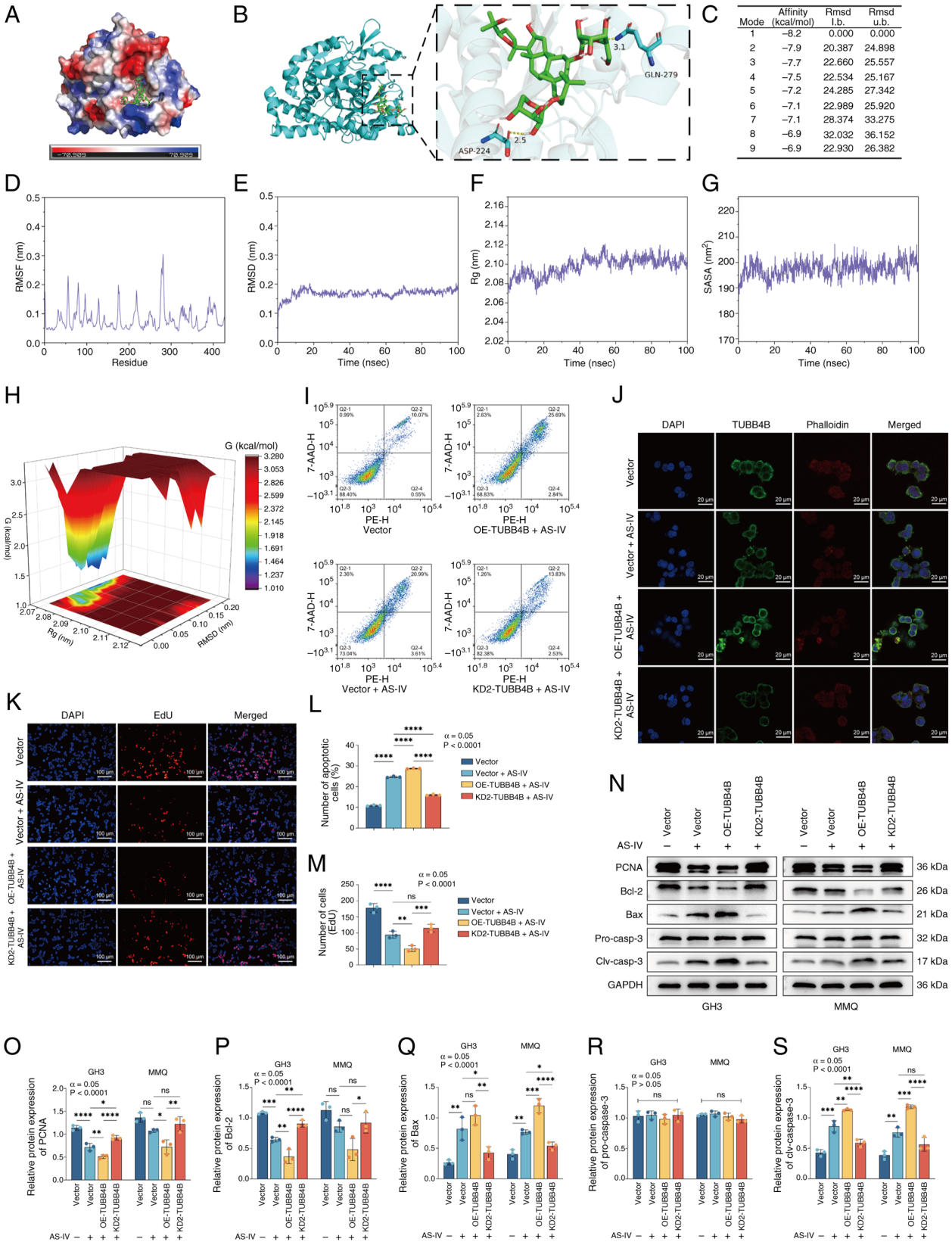

Figure 4. AS-IV exerts an inhibitory effect on pituitary tumors by targeting and binding TUBB4B. (A) Surface electrostatic potential of the TUBB4B protein. (B) Molecular docking between AS-IV (green) and TUBB4B (blue). Yellow dashed lines represent hydrogen bonds. (C) Molecular docking binding energies of AS-IV and TUBB4B in different spatial conformations. (D) RMSF, (E) RMSD, (F) Rg and (G) SASA between TUBB4B protein residues and the AS-IV solution in the experimental system. (H) Free energy landscape showing that the conformation of the AS-IV-TUBB4B complex is dominant and more stable when the Rg was 2.07-2.09 nm and the RMSD was 0.03-0.17 nm. (I) Flow cytometry was used to assess apoptosis of GH3 cells. (J) Immunofluorescence of GH3 cells following AS-IV treatment. (K) EdU staining was used to assess proliferation of GH3 cells. (L) Proportion of apoptotic GH3 cells. (M) Number of EdU-positive cells. (N) Western blotting was used to assess the protein expression of (O) PCNA, (P) Bcl-2, (Q) Bax, (R) pro-caspase-3 and (S) cleaved-caspase-3 in the GH3/MMQ cell lines. ****P<0.0001, ***P<0.001, **P<0.01, *P<0.05. AS-IV, Astragaloside IV; TUBB4B, tubulin beta 4B class IVb; RMSF, root mean square fluctuation; RMSD, Root Mean Square Deviation; Rg, radius of Gyration; SASA, Solvent-Accessible Surface Area; OE, overexpression; KD, knockdown; l. b., lower bound; u. b., upper bound; clv, cleaved; ns, not significant.

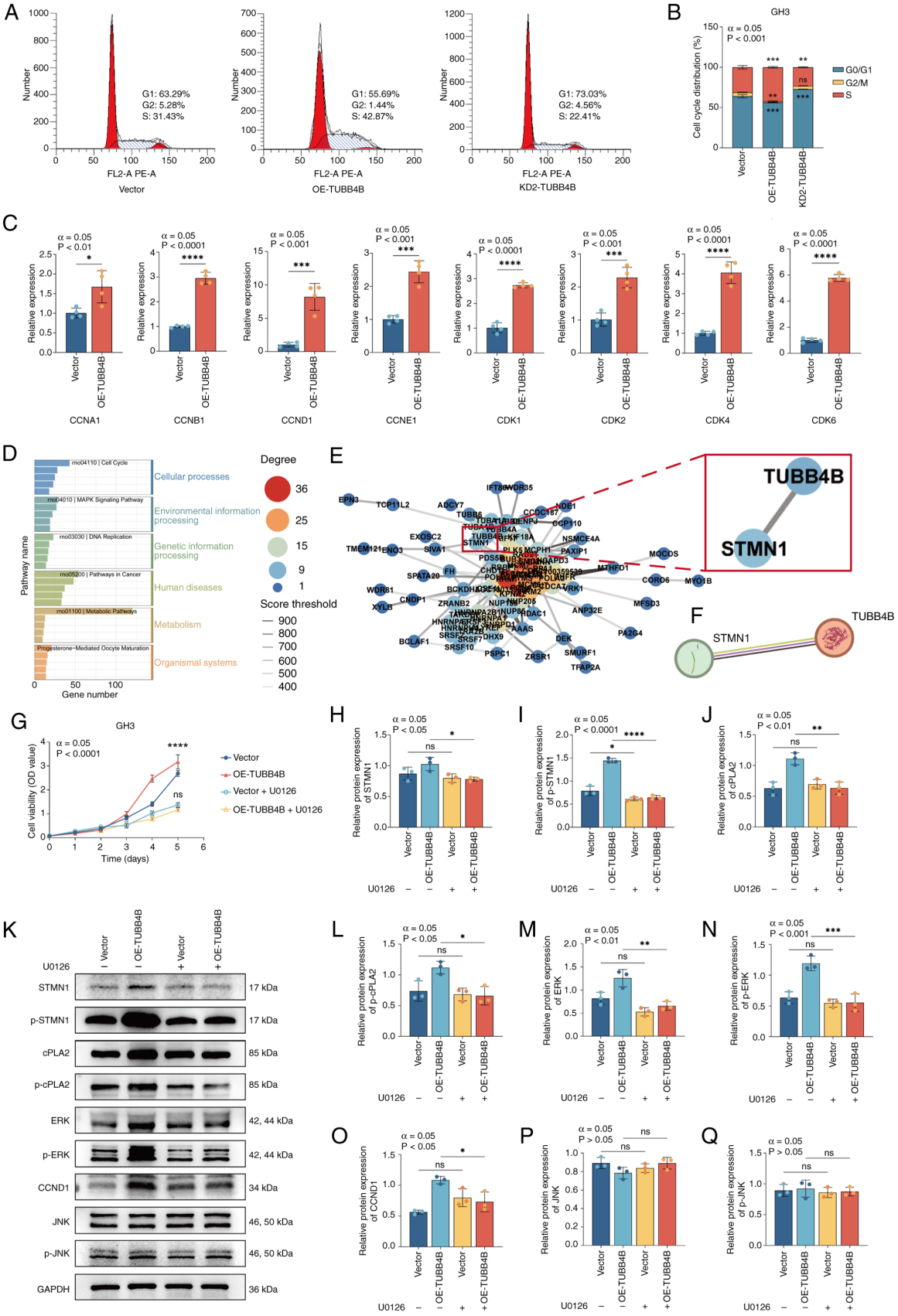

Figure 5. OE-TUBB4B upregulates STMN1 and activates the ERK pathway. (A) Effect of TUBB4B on GH3 cell cycle progression. (B) Cell cycle distribution. (C) Reverse transcription-quantitative PCR was used to assess the effects of OE-TUBB4B. (D) Transcriptomic sequencing showing Kyoto Encyclopedia of Genes and Genomes pathway enrichment of differentially expressed genes. (E) Transcriptomic sequencing showing the protein-protein interaction network of proteins that interact with TUBB4B (red box indicates key pathway proteins that interact with TUBB4B). (F) Interaction diagram between the TUBB4B and STMN1 proteins from STRING. (G) Cell Counting Kit-8 assay was used to assess the viability of GH3 cells treated with U0126. In GH3 cell lines treated with U0126, the protein expression levels of (H) STMN1, (I) p-STMN1 (I), and cPLA2 (J) were assessed by western blotting (K), and levels of p-cPLA2 (L), ERK (M), p-ERK (N), CCND1 (O), JNK (P), and p-JNK (Q) were also assessed. ****P<0.0001, ***P<0.001, **P<0.01, *P<0.05 vs. vector. OE, overexpression; TUBB4B, tubulin beta 4B class IVb; STMN1, stathmin 1; p-, phosphorylated; cPLA2, cytosolic phospholipase A2; CCND1, cyclin D1; KD, knockdown; OD, optical density; ns, not significant.

in the OE-TUBB4B group, whereas they were decreased in the KD2-TUBB4B group (Fig. 6C and C). Compared with the Vector + AS-IV group, both tumor volume and weight were decreased in the OE-TUBB4B + AS-IV group, whereas they were increased in the KD2-TUBB4B + AS-IV group. Overall, the trends in tumor volume and weight were consistent across the groups. The largest tumor was observed in the OE-TUBB4B group, with a maximum tumor diameter of 12.7 mm, a volume of 892 mm^3 and a mass of 1,671 mg. Compared with the shNC group, the OE-TUBB4B group presented notable blood sinuses and the tumor cells exhibited the highest density, large in size, and have a high nucleus-to-cytoplasm ratio, consistent with a state of high proliferation; the KD2-TUBB4B and shNC + AS-IV group presented partial nuclear fragmentation and cytoskeletal fragmentation/degradation in tumor tissue; the OE-TUBB4B + AS-IV group presented notable nuclear pyknosis/fragmentation and severe apoptosis and necrosis of tumor tissue and the KD2-TUBB4B + AS-IV group presented partial nuclear shrinkage but relatively regular tissue morphology (Fig. 6E). Western blotting (Figs. 6F, H-J and S4A-C) and IHC staining (Fig. 6G and K-O) results for the xenograft tumor tissue were consistent with those of the *in vitro* experiments; compared with the Vector group, the OE-TUBB4B group exhibited increased expression of PCNA and Bcl-2 proteins and decreased expression of Bax and cleaved-caspase-3 proteins; while the KD2-TUBB4B group exhibited the opposite trends in these protein expressions compared to the Vector group; Following AS-IV intervention, the OE-TUBB4B+AS-IV group exhibited lower PCNA and Bcl-2 protein expression compared to the Vector + AS-IV group, while Bax and cleaved-caspase-3 protein expression was higher; conversely, the KD2-TUBB4B+AS-IV group showed the opposite trends in these protein expressions compared with the Vector + AS-IV group. These results were consistent with the aforementioned findings that OE-TUBB4B increased the effectiveness of AS-IV, while KD-TUBB4B attenuated effectiveness. Fig. 7 shows the schematic of the overall mechanism by which AS-IV regulates proliferation and apoptosis in pituitary tumors by targeting of TUBB4B. In summary, AS-IV inhibited proliferation and promoted apoptosis of xenograft tumors in animals by targeting of TUBB4B.

Discussion

The present study demonstrated that AS-IV significantly inhibited pituitary tumor cell proliferation and induced apoptosis by targeting TUBB4B and regulating the STMN1/ERK signaling pathway. AS-IV inhibited pituitary tumor cell viability in a concentration- and time-dependent manner, with its molecular mechanism relying on high-affinity binding to TUBB4B and regulation of the downstream STMN1/ERK pathway. To the best of our knowledge, the present study is the first to reveal that TUBB4B OE enhances AS-IV efficacy and TUBB4B regulation affects pituitary tumor cell sensitivity to AS-IV. These findings not only demonstrate the anti-pituitary tumor mechanism of AS-IV but also provide a novel strategy for targeted drug therapy of pituitary tumors and a basis for exploring multitarget regulation by active components in traditional Chinese medicine.

AS-IV, as the primary active component of the traditional Chinese medicine *A. membranaceus*, has advantages for tumor therapy because of its multitarget and low-toxicity characteristics (26). Its ability to inhibit tumor proliferation and invasion while promoting tumor cell apoptosis has been demonstrated both *in vitro* and *in vivo* (27,28). The present study revealed that AS-IV demonstrates enhanced antitumor effects in TUBB4B-overexpressing cells. Molecular docking and kinetic simulations demonstrated that AS-IV bound to TUBB4B with high affinity (binding energy, -8.2 kcal/mol) and formed a stable complex. CETSA confirmed that AS-IV directly bound to TUBB4B and enhanced its thermal stability. Thus, TUBB4B OE may increase the number of intracellular targets available for AS-IV binding, thus increasing the total number of drug-target interactions and overall efficacy. This aligns with the characteristics of AS-IV as a multitarget traditional Chinese medicine component, which exerts stronger effects in target-enriched environments through high-affinity binding (29,30). Second, TUBB4B regulation may be mediated by altering the drug sensitivity of AS-IV. TUBB4B-overexpressing cells exhibited heightened sensitivity to AS-IV (lower IC_{50}), whereas TUBB4B knockdown increased resistance (higher IC_{50}). These findings suggest that TUBB4B expression may serve as a biomarker for AS-IV efficacy, with highly expressing populations potentially benefitting more from AS-IV treatment. Finally, the binding of AS-IV to TUBB4B may disrupt normal interactions between TUBB4B and tubulin or its downstream effector protein STMN1, thus interfering with microtubule dynamics and cell cycle progression. As a key protein in cytoskeletal architecture, TUBB4B directly influences microtubule dynamics and mitotic processes and is associated with cytoskeletal organization and intercellular gap junctions (31). *In vivo* experiments confirmed that AS-IV did not significantly alter TUBB4B protein expression levels, but its proliferation-promoting and apoptosis-inhibiting effects were markedly blocked. These findings suggested that following TUBB4B OE, increased formation of dysfunctional TUBB4B-AS-IV complexes may exacerbate microtubule dysfunction, leading to enhanced proliferation inhibition and apoptosis induction. In summary, the phenomenon of TUBB4B OE enhancing AS-IV efficacy does not contradict conventional targeted therapy logic but reflects the unique mode of action of AS-IV through binding and interfering with target proteins.

The present study used multiomics analysis and experimental validation to demonstrate that TUBB4B activated the ERK pathway by upregulating STMN1 expression, demonstrating its pivotal role in the G1/S transition of the cell cycle. The MAPK pathway comprises four primary branches: ERK, JNK, p38/MAPK and ERK5 (32). Among these pathways, the ERK/MAPK signaling pathway serves as the key network that regulates cell proliferation, development and division (33). STMN1, a key microtubule depolymerizing protein, is upregulated in multiple types of tumor and is associated with poor prognosis; its upregulation accelerates the G1/S transition and promotes proliferation (34). For example, in gallbladder carcinoma, elevated STMN1 expression inhibits tumor growth, induces apoptosis and impairs mitosis (35). In pancreatic cancer, decreased STMN1 expression decreases cell proliferation and invasiveness, while high expression

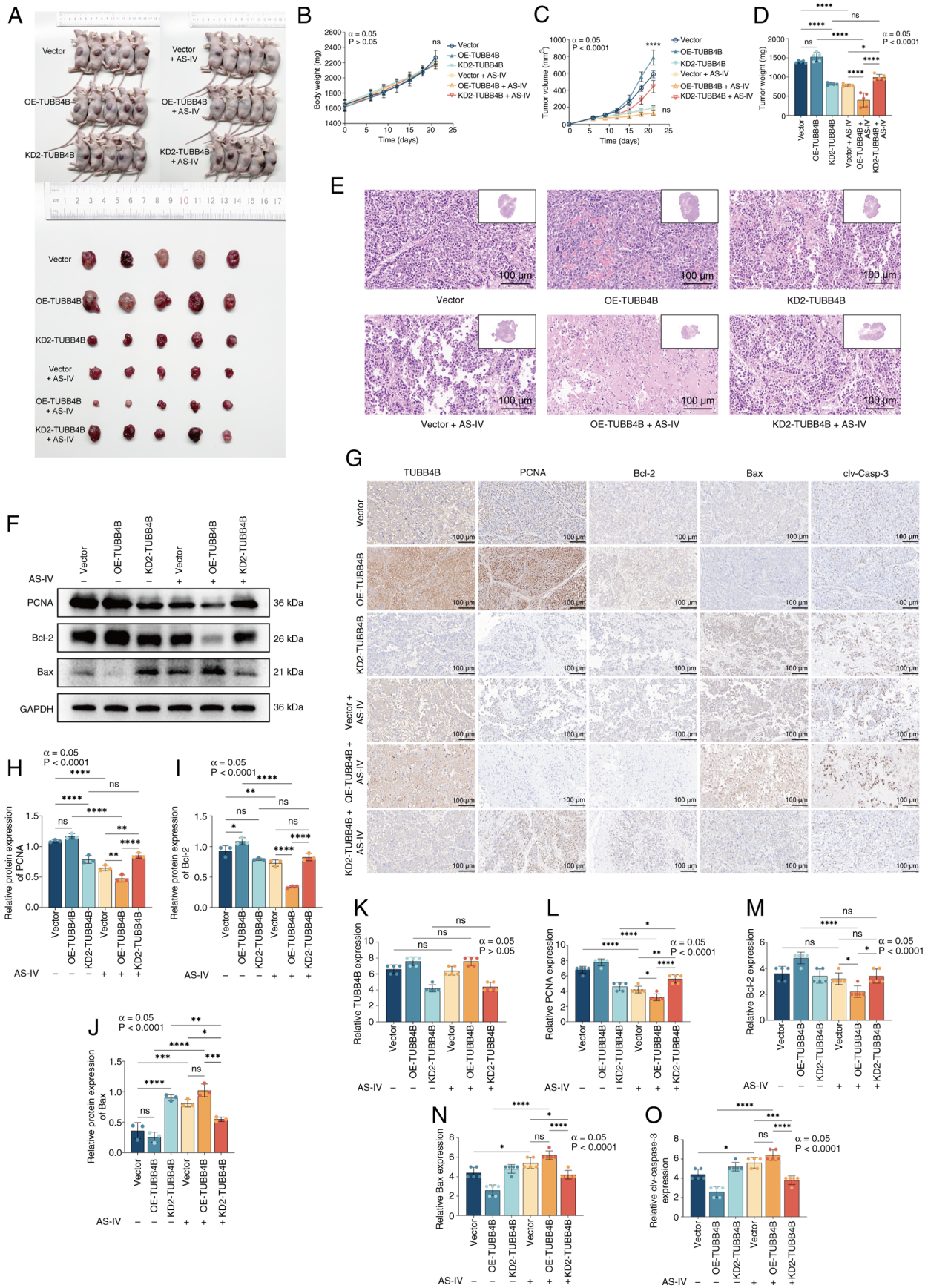

Figure 6. AS-IV inhibits proliferation and promotes apoptosis of xenograft tumors in animals by targeting of TUBB4B. (A) Xenograft tumors in nude mice. (B) Body weight and (C) tumor volume growth curve of the nude mice. (D) Tumor weight. (E) Representative hematoxylin and eosin staining images of tumors (inset: 10X magnification). (F) Western blotting was used to assess protein expression. (G) Representative IHC staining images of TUBB4B, PCNA, Bcl-2, Bax and cleaved-caspase-3 proteins. Expression levels of (H) PCNA, (I) Bcl-2 and (J) Bax. IHC staining scores for (K) TUBB4B, (L) PCNA, (M) Bcl-2, (N) Bax and (O) clv-caspase-3 (Allred scoring system was used). ****P<0.0001, ***P<0.001, **P<0.01, *P<0.05. AS-IV, astragaloside IV; TUBB4B, tubulin β4B class IVb; IHC, immunohistochemistry; OE, overexpression; KD, knockdown; ns, not significant; clv, cleaved.

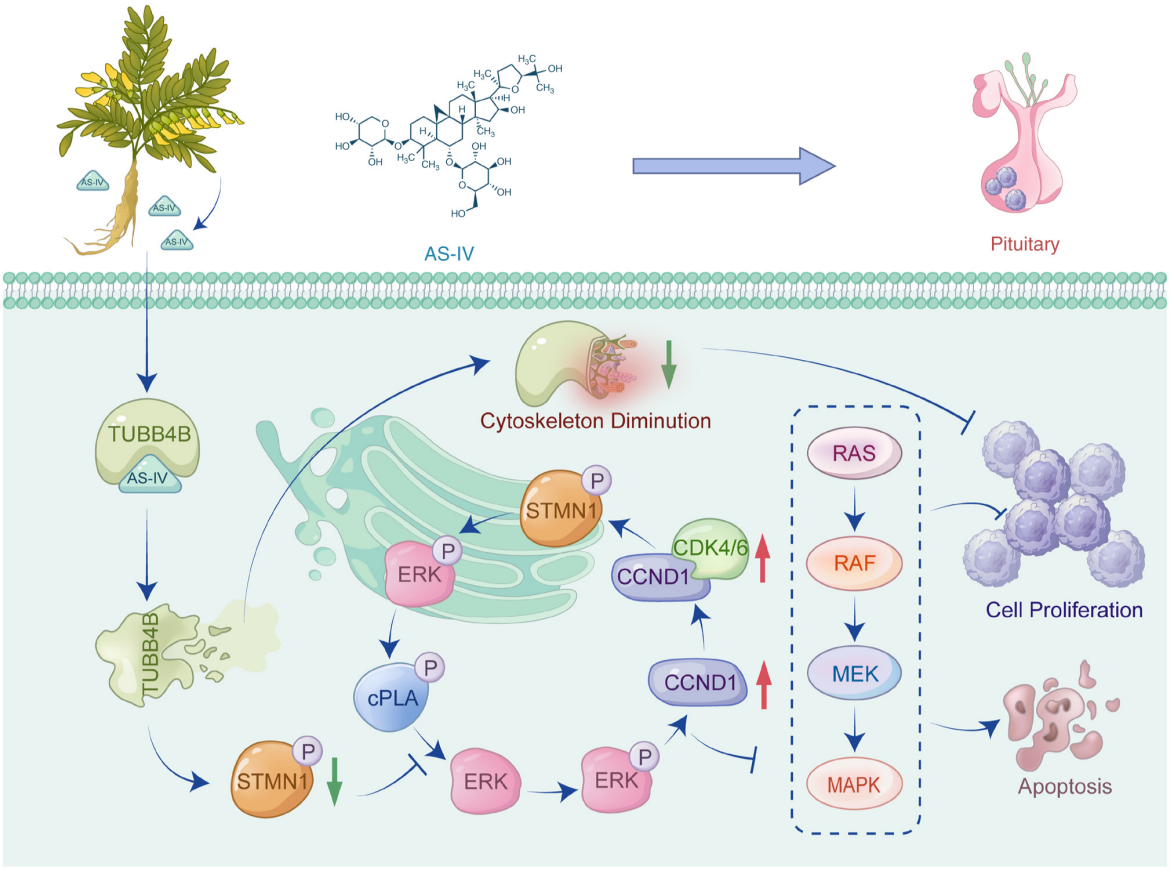

Figure 7. Mechanism by which AS-IV regulates proliferation and apoptosis in pituitary tumors by targeting TUBB4B. AS-IV is chemically purified from the Chinese herbal medicine *Astragalus membranaceus*. AS-IV interacts with pituitary tumor cells by specifically binding TUBB4B, resulting in the formation of a TUBB4B-AS-IV complex. This complex formation decreases cytoskeletal stability while suppressing the expression of the downstream pathway protein STMN1 and its phosphorylation. Additionally, it inhibits the activation of the positive feedback loop of the ERK pathway, suppressing pituitary tumor proliferation and promoting apoptosis. AS-IV, astragaloside IV; TUBB4B, tubulin beta 4B class IVb; cPLA, cytosolic phospholipase A; STMN1, stathmin 1; CCN, cyclin.

promotes distant metastasis and poor differentiation (36). In non-small cell lung cancer, STMN1 upregulation accelerates cell proliferation, regulates microtubule stability to increase migration and invasion and is associated with poor prognosis (37). Inhibiting STMN1 expression and phosphorylation decreases cell proliferation, migration and colony formation capacity (38). In the present study, PPI analysis and immunofluorescence colocalization revealed a physical interaction between TUBB4B and STMN1, with both proteins colocalizing within the microtubule network. Western blotting demonstrated TUBB4B expression significantly affected STMN1 and p-STMN1 expression, accompanied by changes in ERK phosphorylation levels. These findings suggested that TUBB4B may influence STMN1 expression and activity through protein interactions or stability regulation. Following blockade of the ERK pathway with U0126, the proliferation induced by TUBB4B OE was completely reversed, and p-STMN1 and p-ERK levels were not increased, indicating that ERK activation is essential for TUBB4B-mediated proliferation. However, the present study did not modulate the STMN1 gene to validate downstream pathways, nor has it used STMN1-specific inhibitors to rule out the involvement of other pathways. Nevertheless, the results of the KEGG pathway enrichment analysis and cell cycle experiments support the existence of the TUBB4B-STMN1-ERK-cell cycle regulatory axis. Mechanistically, TUBB4B may interact with STMN1 to enhance its phosphorylation and activate the ERK pathway. Activation of ERK increases the total protein expression of cPLA2 and its phosphorylation, which positively feeds back to activate the ERK/MAPK pathway, thus promoting cell proliferation. The effects of STMN1, cPLA2, and ERK pathway proteins have been shown to occur through phosphorylation-mediated activation (39-41). However, the present study found that following regulation by OE-TUBB4B, not only did their phosphorylation levels increase, but their total protein expression also rose. Therefore, it was hypothesized this pathway is subject to feedback' regulation. Nevertheless, the specific mechanisms underlying this regulation have not yet been thoroughly investigated in this study.

Compared with established pituitary tumor drivers such as pituitary-specific transcriptional factor 1, GATA binding protein 2 and ubiquitin specific peptidase 8 (USP8) mutations, TUBB4B is not widely recognized as a key target in pituitary tumors (42-44). However, the present study demonstrated that TUBB4B is highly expressed in pituitary tumors and its regulation significantly affects tumor proliferation and apoptosis, suggesting its potential value as a therapeutic target. Notably, as TUBB4B is a key cytoskeletal protein, TUBB4B inhibitors may exert broad-spectrum antitumor effects by disrupting processes such as mitosis and cell migration. Unlike existing targeted therapies for pituitary tumors, such as dopamine agonists (45) and somatostatin analogs (46), this mechanism

may offer novel therapeutic avenues for drug-resistant or refractory pituitary tumors.

Notably, AS-IV has multiple targeted and multi-pathway effects, which, while advantageous, also introduce complexities and limitations. First, the efficacy of AS-IV varies across different tumor types. Kong *et al* (47) reported an IC_{50} of 100 ng/ml for AS-IV on colorectal cancer cells (47), whereas Qiu *et al* (48) reported a value of 210 μM for uterine leiomyoma cells. Similarly, in the present study, the concentration of AS-IV was also relatively high. This may result from differences in proliferation rate and cell cycle dependency between benign and malignant tumors, variations in the integrity of apoptosis or cell death mechanisms and disparities in the tumor microenvironment and heterogeneity. Second, in addition to regulating the TUBB4B-STMN1-ERK axis, AS-IV may exert antitumor effects through pathways such as the PI3K/Akt (49), NF-κB (50) and TGF-β (51) pathways and induce immune dysfunction (52) and allergic reactions (53) via off-target effects. These pathways and effects exhibit crosstalk with ERK, collectively forming the network pharmacology basis of AS-IV. However, the present study, we did not use drugs with different chemical structures, nor did we conduct additional experiments targeting the same receptor; therefore, we were unable to verify whether off-target effects were present. Future research should integrate proteomics and phosphoproteomics to elucidate the multitarget regulatory landscape of AS-IV in pituitary tumors. Finally, the present study primarily utilized the rat pituitary tumor cell lines GH3 and MMQ, which effectively mimic tumor cell behavior but differ from human pituitary tumor cells in terms of genetic background, molecular phenotype and tumor microenvironment. Future studies should validate the reliability of the TUBB4B-STMN1-ERK axis using human cell lines or primary cell cultures. Additionally, while the present study preliminarily validated the upregulation of TUBB4B in pituitary tumors using clinical samples, the sample size was small and lacked autopsy pituitary specimens for comparative studies. Future studies should incorporate large-scale independent cohort validation and technologies such as tissue microarray to assess the feasibility of TUBB4B as a prognostic biomarker or therapeutic target for pituitary tumors. In summary, targeting TUBB4B by AS-IV may represent a novel adjunctive therapeutic strategy rather than an isolated intervention.

To the best of our knowledge, the present study is the first to demonstrate that AS-IV inhibited pituitary tumor cell proliferation and promoted apoptosis by targeting TUBB4B to suppress the STMN1/ERK signaling pathway. Mechanistically, AS-IV bound TUBB4B with high affinity, enhancing drug sensitivity by blocking downstream STMN1/ERK signaling activation and arresting the cell cycle at G1/S transition phase. TUBB4B OE enhanced AS-IV efficacy, suggesting its potential as a biomarker for AS-IV therapy. The present study not only revealed a novel mechanism underlying the anti-pituitary tumor activity of AS-IV but also provided theoretical support for therapeutic strategies targeting the TUBB4B-STMN1-ERK axis in pituitary tumors.

Acknowledgements

Not applicable.

Funding

The present study was supported by grants from 'Tianshan Talents' Young and Middle-aged Medical and Health Backbone Talents and the 'Science and Technology Program of the Corps' (grant no. 2022CB020).

Availability of data and materials

The data generated in the present study can be accessed at China National GeneBank DataBase under accession number ngb_07871 or at the following URL: db.cngb.org/data_resources/?query=CNP0008409.

Authors' contributions

JL conceived and designed the study, analyzed data and wrote the manuscript. YQ performed molecular docking and visualization. WZ conceived and designed the study. ZY provided experimental guidance and technical support. YZ provided technical support. JX analyzed and interpreted data. KX analyzed data. QL conceived and designed the study and revised the manuscript. JL and QL confirmed the authenticity of all the raw data. All authors have read and approved the final manuscript.

Ethics approval and consent to participate

The present study used anonymized human pituitary tumor tissue and patient data from the First Affiliated Hospital of Shihezi University, with written informed consent obtained from all participants. The human research protocol was approved by the Scientific and Technological Ethics Committee of the First Affiliated Hospital of Shihezi University, Shihezi, China (approval No.: KJ2024-476-01), while the animal experiments were approved by the Bioethics Committee of Shihezi University, Shihezi, China (approval no. A2024-353).

Patient consent for publication

Not applicable.

Competing interests

The authors declare that they have no competing interests.

References

1. Dai C, Kang J, Liu X, Yao Y, Wang H and Wang R: How to classify and define pituitary tumors: Recent advances and current controversies. Front Endocrinol (Lausanne) 12: 604644, 2021.
2. Kong F, Cheng W and Zhan Q: Clinical study on the selection of endoscopes and microscopes for transsphenoidal surgery of non-aggressive pituitary macroadenoma and microadenoma and the influencing factors of hyposmia after endoscopic transsphenoidal surgery. Front Neurol 15: 1321099, 2024.
3. Raverot G, Ilie MD, Lasolle H, Amodru V, Trouillas J, Castinetti F and Brue T: Aggressive pituitary tumours and pituitary carcinomas. Nat Rev Endocrinol 17: 671-684, 2021.
4. Burman P, Casar-Borota O, Perez-Rivas LG and Dekkers OM: Aggressive pituitary tumors and pituitary carcinomas: From pathology to treatment. J Clin Endocrinol Metab 108: 1585-1601, 2023.

5. Raverot G and Ilie MD: Immunotherapy in pituitary carcinomas and aggressive pituitary tumors. Best Pract Res Clin Endocrinol Metab 36: 101712, 2022.
6. Liang Y, Chen B, Liang D, Quan X, Gu R, Meng Z, Gan H, Wu Z, Sun Y, Liu S and Dou G: Pharmacological effects of astragaloside IV: A review. Molecules 28: 6118, 2023.
7. Xia D, Li W, Tang C and Jiang J: Astragaloside IV, as a potential anticancer agent. Front Pharmacol 14: 1065505, 2023.
8. Li L, Li G, Chen M and Cai R: Astragaloside IV enhances the sensibility of lung adenocarcinoma cells to bevacizumab by inhibiting autophagy. Drug Dev Res 83: 461-469, 2021.
9. Zhu Y and Lu F: Astragaloside IV inhibits cell viability and glycolysis of hepatocellular carcinoma by regulating KAT2A-mediated succinylation of PGAM1. BMC Cancer 24: 682, 2024.
10. Yu Y, Hao J, Wang L, Zheng X, Xie C, Liu H, Wu J, Qiao S and Shi J: Astragaloside IV antagonizes the malignant progression of breast cancer induced by macrophage M2 polarization through the TGF-β-regulated Akt/Foxo1 pathway. Pathol Res Pract 249: 154766, 2023.
11. Dharmapal D, Jyothy A, Mohan A, Balagopal PG, George NA, Sebastian P, Maliekal TT and Sengupta S: β-Tubulin isotype, TUBB4B, regulates the maintenance of cancer stem cells. Front Oncol 11: 788024, 2021.
12. Feng M, Wang K, Fu S, Wei H, Mu X, Li L and Zhang S: Tubulin TUBB4B Is involved in spermatogonia proliferation and cell cycle processes. Genes (Basel) 13: 1082, 2022.
13. Yang Y, Boza-Serrano A, Dunning CJR, Clausen BH, Lambertsen KL and Deierborg T: Inflammation leads to distinct populations of extracellular vesicles from microglia. J Neuroinflammation 15: 168, 2018.
14. McFadden JR, Tolete CDP, Huang Y, Macnamara E, Sept D, Nesterova G, Gahl WA, Sackett DL and Malicdan MCV: Clinical, genetic, and structural characterization of a novel TUBB4B tubulinopathy. Mol Genet Metab Rep 36: 100990, 2023.
15. Hu H, Zhang Y, Zhai H, Dong J, Zuo L, Guo X and Wang C: P300 reduces TUBB4B expression to facilitate the biological process of migration and invasion of non-small cell lung cancer cells. Tissue Cell 88: 102386, 2024.
16. Zhang W, Zhang P, Pu Y, Chen Z, Su G, Deng Y, Zhang Y, Ji Y, Huang Z, Zhou Q, *et al*: DNA 5-hydroxymethylcytosine landscape and transcriptional profile highlight the TUBB4B-mediated Th17/Th1/Treg imbalance in Behçet's uveitis. Invest Ophthalmol Vis Sci 66: 28, 2025.
17. Sobierajska K, Ciszewski WM, Wawro ME, Wieczorek-Szukała K, Boncela J, Papiewska-Pajak I, Niewiarowska J and Kowalska MA: TUBB4B downregulation is critical for increasing migration of metastatic colon cancer cells. Cells 8: 810, 2019.
18. Filipovich E, Gorodkova E, Shcherbakova A, Asaad W, Popov S, Melnichenko G, Mokrysheva N and Utkina M: The role of cell cycle-related genes in the tumorigenesis of adrenal and thyroid neuroendocrine tumors. Heliyon 11: e41457, 2024.
19. Liu B, Wang J, Wang G, Jiang W, Li Z, Shi Y, Zhang J, Pei Q, Huang G, Wang L, *et al*: Hepatocyte-derived exosomes deliver H2AFJ to hepatic stellate cells and promote liver fibrosis via the MAPK/STMN1 axis activation. Int Immunopharmacol 115: 09605, 2023.
20. Wang C, Zhang H, Xu F, Niu Y, Wu Y, Wang X, Peng Y, Sun J, Liang L and Xu P: Substituted 3-benzylcoumarins as allosteric MEK1 inhibitors: Design, synthesis and biological evaluation as antiviral agents. Molecules 18: 6057-6091, 2013.
21. Livak KJ and Schmittgen TD: Analysis of relative gene expression data using real-time quantitative PCR and the 2(-Delta Delta C(T)) method. Methods 25: 402-408, 2001.
22. Elking DM: A non-periodic particle mesh Ewald method for radially symmetric kernels in free space. Comput Phys Commun 312: 109739, 2025.
23. Bussi G, Donadio D and Parrinello M: Canonical sampling through velocity rescaling. J Chem Phys 126: 014101, 2007.
24. Hosseini AN and van der Spoel D: Martini on the rocks: Can a coarse-grained force field model crystals? J Phys Chem Lett 15: 1079-1088, 2024.
25. Zocchi R, Compagnucci C, Bertini E and Sferra A: Deciphering the tubulin language: Molecular determinants and readout mechanisms of the tubulin code in neurons. Int J Mol Sci 24: 2781, 2023.
26. Liu X, Chu W, Shang S, Ma L, Jiang C, Ding Y, Wang J, Zhang S and Shao B: Preliminary study on the anti-apoptotic mechanism of astragaloside IV on radiation-induced brain cells. Int J Immunopathol Pharmacol 34: 2058738420954594, 2020.
27. Hu T, Fei Z and Wei N: Chemosensitive effects of astragaloside IV in osteosarcoma cells via induction of apoptosis and regulation of caspase-dependent Fas/FasL signaling. Pharmacol Rep 69: 1159-1164, 2017.
28. Liu J, Wang D, Ren N, Zhang L and Wang T: Metabolites of *Astragalus membranaceus* and their pro-apoptotic and cytotoxic activities: Insights into targeted metabolic pathways. Front Pharmacol 16: 1647958, 2025.
29. Wu M, Li K, Wu J, Zhang Q, Ma X, Dai W, Gao H, Ding X, Wang W and Xiao W: Astragaloside IV: A multipotent phytochemical for treating fibrotic diseases (Review). Int J Mol Med 57: 50, 2026.
30. Xu L, Li Y, He Z, Chen W and Li Y: Astragaloside IV ameliorates experimental autoimmune myasthenia gravis through multi-target regulation of immune-microbiota-metabolism network and ferroptosis inhibition. Pathol Res Pract: Feb 24, 2026 (Epub ahead of print).
31. Sanzhaeva U, Wonsettler NR, Rhodes SB and Ramamurthy V: TUBB4B is essential for the expansion of differentiating spermatogonia. Sci Rep 14: 20889, 2024.
32. Fang Z, Meng Q, Xu J, Wang W, Zhang B, Liu J, Liang C, Hua J, Zhao Y, Yu X and Shi S: Signaling pathways in cancer-associated fibroblasts: Recent advances and future perspectives. Cancer Commun (Lond) 43: 3-41, 2023.
33. Guo YJ, Pan WW, Liu SB, Shen ZF, Xu Y and Hu LL: ERK/MAPK signalling pathway and tumorigenesis. Exp Ther Med 19: 1997-2007, 2020.
34. Zhang X, Ji J, Yang Y, Zhang J and Shen L: Stathmin1 increases radioresistance by enhancing autophagy in non-small-cell lung cancer cells. Onco Targets Ther 9: 2565-2574, 2016.
35. Wang S, Su T, Tong H, Zhou D, Ma F, Ding J, Hao Y, Shi W and Quan Z: Circβ-catenin promotes tumor growth and Warburg effect of gallbladder cancer by regulating STMN1 expression. Cell Death Discov 7: 233, 2021.
36. Li J, Kong F, Wu K, Song K, He J and Sun W: miR-193b directly targets STMN1 and uPA genes and suppresses tumor growth and metastasis in pancreatic cancer. Mol Med Rep 10: 2613-2620, 2014.
37. Zeng L, Lyu X, Yuan J, Chen Y, Wen H, Zhang L, Shi J, Liu B, Li W and Yang S: STMN1 promotes tumor metastasis in non-small cell lung cancer through microtubule-dependent and nonmicrotubule-dependent pathways. Int J Biol Sci 20: 1509-1527, 2024.
38. Li M and Zhou Q: Prognostic value of STMN1 expression in non-small cell lung cancer: A Meta-analysis. Zhongguo Fei Ai Za Zhi 27: 826-830, 2024 (In Chinese).
39. Zhang Y, Wei S, Zhang Q, Zhang Y and Sun C: Paris saponin VII inhibits triple-negative breast cancer by targeting the MEK/ERK/STMN1 signaling axis. Phytomedicine 130: 155746, 2024.
40. Lovrić J, Dammeier S, Kieser A, Mischak H and Kolch W: Activated raf induces the hyperphosphorylation of stathmin and the reorganization of the microtubule network. J Biol Chem 273: 22848-22855, 1998.
41. Ye Y, Liu L, Feng Z, Liu Y, Miao J, Wei X, Li H, Yang J, Cao X and Zhao J: The ERK-cPLA2-ACSL4 axis mediating M2 macrophages ferroptosis impedes mucosal healing in ulcerative colitis. Free Radic Biol Med 214: 219-235, 2024.
42. Wang X, Li J, Jiang C, Zhang C, Yuan L, Zhang T, Liu Y, Ma S, Kang P, Li D, *et al*: Splicing factor FUS facilitates the progression of PIT1-lineage PitNETs by upregulating MDM2. Theranostics 16: 3032-3049, 2026.
43. Mitsutani M, Matsushita M, Yokoyama M, Morita A, Hano H, Fujikawa T, Tagami T and Moriyama K: Growth hormone directly stimulates GATA2 expression. Growth Horm IGF Res 74: 101572, 2024.
44. Zhou W, Zheng S, Ye L, Su T, Xie J, Jiang L, Jiang Y, Zhong X, Wu L, Zhou W and Wang W: The USP8 mutational status in combination with postsurgical cortisol levels for predicting recurrence of cushing disease. J Clin Endocrinol Metab 111: e156-e165, 2025.
45. Kaparounaki C, Ilie MD, De Alcubierre D, Anagnostis P, Haidich AB, Isidori AM, Dekkers OM, Goulis DG and Raverot G: Medical treatment in acromegaly: A network meta-analysis. Eur J Endocrinol 193: S83-S94, 2025.
46. He D, Wang Q, Sheng Z and Li G: Preoperative medical therapy for acromegaly: Current knowledge and clinical significance. Front Endocrinol (Lausanne) 16: 1636047, 2026.
47. Kong P, Tang X, Liu F and Tang X: Astragaloside IV regulates circ_0001615 and miR-873-5p/LASP1 axis to suppress colorectal cancer cell progression. Chem Biol Drug Des 103: e14423, 2024.

48. Qiu T, Li D, Liu Y, Ren H, Yang X and Luo W: Astragaloside IV inhibits the proliferation of human uterine leiomyomas by targeting IDO1. Cancers (Basel) 14: 4424, 2022.
49. Zhang X, Zhang F, Li Y, Fan N, Zhao K, Zhang A, Kang J, Lin Y, Xue X and Jiang X: Blockade of PI3K/AKT signaling pathway by astragaloside IV attenuates ulcerative colitis via improving the intestinal epithelial barrier. J Transl Med 22: 406, 2024.
50. Li M, Niu Y, Tian L, Zhang T, Zhou S, Wang L, Sun J, Wumiti T, Chen Z, Zhou Q, *et al*: Astragaloside IV alleviates macrophage senescence and d-galactose-induced bone loss in mice through STING/NF-κB pathway. Int Immunopharmacol 129: 111588, 2024.
51. Li L, Wang Q, He Y, Sun L, Yang Y and Pang X: Astragaloside IV suppresses migration and invasion of TGF-β_1-induced human hepatoma HuH-7 cells by regulating Nrf2/HO-1 and TGF-β_1/Smad3 pathways. Naunyn Schmiedebergs Arch Pharmacol 395: 397-405, 2022.
52. Yu Z, Gao M, Wu X, Li J, Liu B, Wang R, Tan J, Yu X and Geng L: Potential mechanisms and effects of AFB1-induced asthma: A comprehensive analysis based on network toxicology and molecular docking. PLoS One 21: e0341172, 2026.
53. Zou F, Du Q, Zhang Y, Zuo L and Sun Z: Pseudo-allergic reactions induced by Chinese medicine injections: A review. Chin Med 18: 149, 2023.